# Model Predictive Control of a Modular Multilevel Converter Considering Control Input Constraints

Xiaonan Gao, *Member, IEEE*, Wei Tian, *Member, IEEE*, Qifan Yang, *Member, IEEE*, Na Chai, *Member, IEEE*, Jose Rodriguez, *Life Fellow, IEEE*, Ralph Kennel, *Life Senior Member, IEEE*, and Marcelo Lobo Heldwein, *Senior Member, IEEE*

***Abstract*—Model predictive control (MPC) usually suffers from high computational complexity when it comes to modular multilevel converters (MMCs). Some researchers have attempted to use a modulated approach to reduce the computational burden and improve the control performance. But these methods do not consider the actual physical limitations of the control system, and therefore the control performance degrades at high modulation indices or transients. To solve this problem, a modulated MPC with bound-constrained quadratic programming has been proposed. With this method, the optimal solution of the control problem can be obtained, ensuring a better control performance under high modulation index conditions or in transients. Finally, a comparative experiment with the conventional modulated MPC methods has been carried out. The experimental results validate that the proposed method can achieve superior performance when the MMC operates at high modulation index, transients, and low frequencies.**

***Index Terms*—Model predictive control (MPC), modular multilevel converters (MMCs), quadratic programming (QP), simple bounds.**

## I. Introduction

OVER the past decade, modular multilevel converters (MMCs) have attracted increasing attention in the medium- and high-voltage applications [1]. In comparison with other multilevel converters, MMC shows better scalability and modularity, which can achieve a very low total harmonic distortion (THD) of output currents and switching frequency [2]. Due to these excellent features, it becomes more and more popular in high-voltage direct current transmission systems [3], static synchronous compensator [4], and medium voltage (MV) motor drives [5].

Although MMC has many advantages, its control structure is usually complex. To achieve multiobjective control, cascaded or paralleled control structures with proportional-integral controllers and/or proportional-resonant controllers [6] are typically adopted in traditional methods. However, these linear controllers usually result in slow dynamic response and narrow bandwidth [7]. Besides, the complicated control structure of the MMC system further increases the difficulty of the control system design.

Recently, model predictive control (MPC) has emerged as a common and efficient technique in the field of power electronics and motor drives due to its fast-dynamic response, capability for the control of multiple variables, easy inclusion of constraints [8], [9]. Because of its successful application in other voltage-source converters, MPC has drawn more attention as an alternative control scheme in MMC systems.

The mathematical model of the MMC is the foundation for the control designs, especially for MPC. Generally speaking, two models, per-phase model [10], [11], [12] and three-phase model [13], [14], [15], [16], are widely adopted in MPC schemes. With the per-phase model, each phase of MMC can be controlled independently, which obviously simplifies the control design process and reduces the computational complexity. However, the underlying assumption for using the per-phase model is that the common-mode voltage during each control cycle is 0. This requirement is not always satisfied with the per-phase model-based method, which leads to a slight degradation of control performance [15]. Instead, the MPC method based on the three-phase model, as it considers the effect of the common-mode voltage, can achieve better steady-state performance. Moreover, ac-side currents, circulating currents, and dc-link current/voltage can be controlled independently with the three-phase model. However, due to its control and computational complexity, the three-phase model-based method is usually applied to MMCs with fewer submodules per arm.

Based on whether modulation techniques are adopted, MPC schemes for MMCs are classified into finite control set (FCS)-MPC-based methods [10], [11], [17] and modulated MPC methods [16], [18], [19]. Due to its straightforward control structure, fast dynamic response and low switching frequency under high sampling frequency, FCS-MPC was first applied to MMC in academia [10]. In this method, the MPC controller has been

Manuscript received 24 February 2023; revised 18 August 2023; accepted 18 September 2023. Date of publication 22 September 2023; date of current version 6 December 2023. This work was supported in part by the Deutsche Forschungsgemeinschaft (DFG, German Research Foundation) under Grant 432509817, and in part by the ANID under Grants FB0008, 1210208, and 1221293. Recommended for publication by Associate Editor. *(Corresponding author: Wei Tian.)*

Xiaonan Gao is with the Division of Electric Power and Energy Systems, KTH Royal Institute of Technology, 10044 Stockholm, Sweden (e-mail: xiaonan@kth.se).

Wei Tian, Qifan Yang, Ralph Kennel, and Marcelo Lobo Heldwein are with the Chair of High-Power Converter Systems, Technical University of Munich, 80333 Munich, Germany (e-mail: wei.tian@tum.de; qifan.yang@tum.de; ralph.kennel@tum.de; marcelo.heldwein@tum.de).

Na Chai is with the College of Electronic and Information Engineering, Hunan University, Changsha 410082, China (e-mail: nachai@hnu.edu.cn).

Jose Rodriguez is with the Faculty of Engineering, Universidad San Sebastian, Santiago 8420497, Chile (e-mail: jose.rodriguezp@uss.cl).

Color versions of one or more figures in this article are available at https://doi.org/10.1109/TPEL.2023.3318320.

Digital Object Identifier 10.1109/TPEL.2023.3318320

used to control the output ac currents, SM capacitor voltages, and circulating currents by evaluating all the $C_{2N}^{N}$ possible insertion index combinations per phase, in which $N$ is the number of SMs in each arm. However, the number of enumerated combinations of this method increases significantly when $N$ increases, which leads to a huge computational burden. To overcome the high computational burden brought by FCS-MPC, many researchers have adopted the per-phase model of the MMC and proposed some heuristic methods. In [11], an indirect FCS-MPC scheme for MMCs has been proposed. This method only needs to obtain the number of the inserted SMs in each arm and uses an external voltage sorting algorithm to balance the SM capacitor voltages in the same arm. The total number of the enumerated combinations of this scheme decreases to $(N+1)^2$ in each phase. The computational burden can be further reduced by reasonably limiting the selection range of the possible insertion index combinations [12], [20]. However, the dynamic performance of these methods will be influenced due to the sacrifice of a large number of the possible insertion index combinations. In [21], a proper selection of insertion indices can be determined by solving a quadratic programming (QP) problem. Unfortunately, this method is only applicable to the per-phase model-based MPC. The research on the three-phase model-based FCS-MPC method can be found in [13], [14]. In [14], a dual-stage MPC scheme for MMCs has been proposed to reduce the computational complexity. This method needs to evaluate $(N+1)^3$ switching vectors at first stage and $C_N^{N/2}$ switching states per arm at the second stage.

In addition to the studies on FCS-MPC methods, some scholars have turned to use the modulated MPC technique for the MMC system to further reduce the computational burden and improve steady-state performance [16], [18], [19], [22]. The method introduced in [18] is similar to the per-phase model-based FCS-MPC method. It first selects two optimal adjacent voltage levels based on the cost function. The duty cycles of these two voltage levels can be calculated in each control period. Although the steady-state performance can be improved by using this method, there are still $(N+1)$ voltage levels per phase that need to be evaluated. The modulated MPC methods introduced in [16], [19], [22] share a similar principle, whose essence is deadbeat control, and in this work, these methods can be equivalent to solving an unconstrained solution to a quadratic optimization problem (cost function). In [19], [22], the per-phase model has been applied so that low control complexity can be achieved. The steady-state performance of these methods has been improved compared with FCS-MPC methods under the same sampling frequency. In addition, with such methods, the computational burden is independent of $N$ and thus is extremely low. However, these methods cannot directly control the common-mode voltage, so they are not suitable for MMC-based MV motor drives. Instead, the method proposed in [16] is based on the three-phase model and it therefore has the capability to directly control the common-mode voltage and dc-link voltage/current. However, all these schemes [16], [19], [22] do not take into account the case when the obtained unconstrained solution exceeds the physical limits of the MMC system. Note that in this case, the weighting factor will have a significant impact on the control system. Unfortunately, these methods ignore this effect. And in such a situation, using the unconstrained solution does not prioritize the performance of the most important control objectives. As a result, the control performance will deteriorate when the MMC is operating at a high modulation index or during transients (in these cases the unconstrained solution may exceed the limit).

To solve the abovementioned problems, an MPC method based on bound-constrained QP is proposed. At first, the control problem for the MMC system based on the MPC method has been formulated as a QP problem with simple bounds. After that, an infeasible active-set method [23] has been employed to quickly obtain the optimal solution of this control problem. Then, the obtained solution can be used to implement the modulated MPC scheme. It can be seen that the proposed method retains the advantage of computational efficiency that the conventional modulated methods have, since the computational burden is independent of $N$. Compared to the conventional modulated MPC schemes [16], [19], [22], due to the use of optimal solution, the proposed method can provide a better control performance when the MMC operates at high modulation indices or transients. In addition, the proposed method is more suitable for the MMC-based MV motor drives, not only because it applies the three-phase model, but also because the MMC system will often be in transients under such applications.

The main contributions of this work can be summarized as follows.

1) This article reveals that the conventional modulated MPC methods in [16], [19], [22] can be regarded as solving the unconstrained solution to a control problem and thus cannot guarantee a good control performance of the MMC system when the constraints of the control input are violated.
2) To further enhance the control performance of the modulated MPC method, we adopt a QP method to find the optimal solution of the control problem. Unlike the conventional method that uses an unconstrained solution followed by saturation, using the optimal solution allows prioritizing the control performance of the most important control objectives, resulting in better control performance of the system.

The rest of this article is organized as follows. The mathematical model of the MMC is presented in Section II. The conventional modulated MPC method and the proposed method are presented in Section III. The comparative experimental results are provided in Section IV. Finally, Section V concludes this article.

## II. Mathematical Model of the MMC

Fig. 1 shows the topological structure of a three-phase MMC. It can be seen that the MMC has three legs, and each leg contains two arms (upper and lower arm). Each arm is constructed with $N$ cascaded SMs and an arm inductor $L$ (neglecting the resistance of the inductor). "O" is the virtual midpoint of dc-link and "N" is the neutral point of the ac side. $i_{\mathrm{ua}}$, $i_{\mathrm{la}}$, $i_{\mathrm{ub}}$, $i_{\mathrm{lb}}$, $i_{\mathrm{uc}}$, and $i_{\mathrm{lc}}$ are

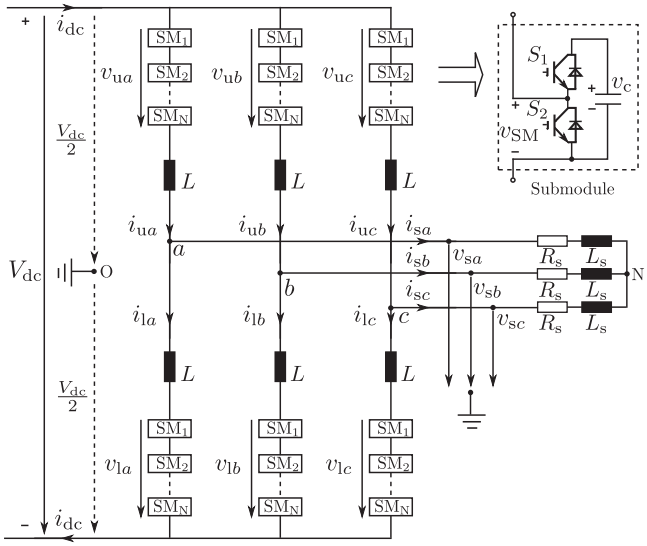


Fig. 1. Configuration of a three-phase MMC.

the currents flowing through the upper and lower arms in three phases, respectively. $v_{ua}$, $v_{la}$, $v_{ub}$, $v_{lb}$, $v_{uc}$, and $v_{lc}$ represent the voltages produced by the upper and lower arms in three phases, respectively. $v_{sa}$, $v_{sb}$, and $v_{sc}$ are the equivalent ac-side output voltages of the MMC. $V_{dc}$ and $i_{dc}$ are the dc-link voltage and current, respectively.

The control variables concerning about the current can be divided into three parts: ac-side currents, dc-link current, and circulating currents. The ac-side currents can be obtained with

$$i_{sx} = i_{ux} - i_{lx},\ x = a, b, c. \tag{1}$$

The dc-link current is given by

$$i_{dc} = \sum_{x=a,b,c} i_{ux} = \sum_{x=a,b,c} i_{lx}. \tag{2}$$

The circulating currents are defined as

$$i_{zx} = \frac{i_{ux} + i_{lx}}{2} - \frac{i_{dc}}{3},\ x = a, b, c. \tag{3}$$

It is worth noting that the sum of the circulating currents is zero, which means that the circulating currents flow only among the three legs of the converter without being leaked to the ac side and the dc-link side.

According to Kirchhoff's voltage law, the upper and lower arm voltages with respect to the midpoint of the dc-link can be obtained as

$$\begin{aligned} \frac{V_{dc}}{2} &= v_{ux} + L\frac{di_{ux}}{dt} + R_s i_{sx} + L_s\frac{di_{sx}}{dt} + v_{NO} \\ \frac{V_{dc}}{2} &= v_{lx} + L\frac{di_{lx}}{dt} - R_s i_{sx} - L_s\frac{di_{sx}}{dt} - v_{NO}. \end{aligned} \tag{4}$$

It should be noted that $v_{NO}$ is the common mode voltage, which represents the voltage potential between the neutral point "N" and dc bus virtual midpoint "O."

Based on (1)–(4), the dynamics of three-phase ac-side currents, circulating currents, and dc-link current can be derived as

$$\begin{aligned} \frac{d\boldsymbol{i}_s}{dt} &= \frac{1}{2L_s + L}\left(\boldsymbol{v}_l - \boldsymbol{v}_u - 2\boldsymbol{v}_{NO} - 2R_s\boldsymbol{i}_s\right) \\ \frac{d\boldsymbol{i}_z}{dt} &= \frac{1}{2L}\left(\boldsymbol{v}_{sum} - \boldsymbol{v}_l - \boldsymbol{v}_u\right) \\ \frac{di_{dc}}{dt} &= \frac{3}{2L}\left(V_{dc} - v_{sum}\right) \end{aligned} \tag{5}$$

where

$$\boldsymbol{i}_s = \begin{bmatrix} i_{sa} \\ i_{sb} \\ i_{sc} \end{bmatrix},\quad \boldsymbol{v}_l = \begin{bmatrix} v_{la} \\ v_{lb} \\ v_{lc} \end{bmatrix},\quad \boldsymbol{v}_u = \begin{bmatrix} v_{ua} \\ v_{ub} \\ v_{uc} \end{bmatrix}$$

$$\boldsymbol{i}_z = \begin{bmatrix} i_{za} \\ i_{zb} \\ i_{zc} \end{bmatrix},\quad \boldsymbol{v}_{NO} = \begin{bmatrix} v_{NO} \\ v_{NO} \\ v_{NO} \end{bmatrix},\quad \boldsymbol{v}_{sum} = \begin{bmatrix} v_{sum} \\ v_{sum} \\ v_{sum} \end{bmatrix}$$

$v_{NO} = \frac{1}{6}\sum_{x=a,b,c}(v_{lx} - v_{ux})$, $v_{sum} = \frac{1}{3}\sum_{x=a,b,c}(v_{lx} + v_{ux})$.

The arm voltages ($v_{ux}$ and $v_{lx}$) can be expressed as

$$\begin{aligned} v_{ux} &= \frac{n_{ux}}{N}\sum_{i=1}^{N} v_{c,ux}^i = n_{ux}\bar{v}_{ux} \\ v_{lx} &= \frac{n_{lx}}{N}\sum_{i=1}^{N} v_{c,lx}^i = n_{lx}\bar{v}_{lx} \end{aligned} \tag{6}$$

where $n_{yx}$ ($y = u, l$ and $x = a, b, c$) is the number of inserted SMs in upper/lower arm (also called insertion index). $v_{c,ux}^i$ and $v_{c,lx}^i$ are the voltage of the capacitor in $i$th SM in upper and lower arms of phase $x$. $\bar{v}_{yx}$ is the average capacitor voltage in arm $y$ of phase $x$. Here, we assume that the capacitor voltage of each SM in the same arm is well balanced due to the voltage sorting algorithm.

By using the forward Euler method for (5), the discrete-time domain mathematical model can be obtained as

$$\begin{aligned} \boldsymbol{i}_s(k+1) &= \alpha_1\boldsymbol{i}_s(k) + \alpha_2\left(\boldsymbol{v}_l(k) - \boldsymbol{v}_u(k) - 2\boldsymbol{v}_{NO}(k)\right) \\ \boldsymbol{i}_z(k+1) &= \boldsymbol{i}_z(k) + \alpha_3\left(\boldsymbol{v}_{sum}(k) - \boldsymbol{v}_l(k) - \boldsymbol{v}_u(k)\right) \\ i_{dc}(k+1) &= i_{dc}(k) + 3\alpha_3\left(V_{dc} - v_{sum}(k)\right) \end{aligned} \tag{7}$$

where

$$\alpha_1 = 1 - \frac{2R_sT_s}{2L_s + L}, \alpha_2 = \frac{T_s}{2L_s + L}, \alpha_3 = \frac{T_s}{2L}$$

$$\boldsymbol{v}_u(k) = \begin{bmatrix} n_{ua}\bar{v}_{ua} & n_{ub}\bar{v}_{ub} & n_{uc}\bar{v}_{uc} \end{bmatrix}^T$$

$$\boldsymbol{v}_l(k) = \begin{bmatrix} n_{la}\bar{v}_{la} & n_{lb}\bar{v}_{lb} & n_{lc}\bar{v}_{lc} \end{bmatrix}^T$$

$$v_{sum}(k) = \frac{1}{3}\begin{bmatrix} 1 & 1 & 1 \end{bmatrix}\left(\boldsymbol{v}_l(k) + \boldsymbol{v}_u(k)\right)$$

$$v_{NO}(k) = \frac{1}{6}\begin{bmatrix} 1 & 1 & 1 \end{bmatrix}\left(\boldsymbol{v}_l(k) - \boldsymbol{v}_u(k)\right)$$

and $T_s$ is the sampling interval.

According to (7), the discrete-time mathematical model in the linear matrix form can be obtained as

$$\boldsymbol{y} = \boldsymbol{A}\boldsymbol{x} + \boldsymbol{b} \tag{8}$$

where

$$\boldsymbol{y} = \begin{bmatrix} i_{\mathrm{s}a}(k+1) \\ i_{\mathrm{s}b}(k+1) \\ i_{\mathrm{s}c}(k+1) \\ i_{\mathrm{z}a}(k+1) \\ i_{\mathrm{z}b}(k+1) \\ i_{\mathrm{z}c}(k+1) \end{bmatrix}, \boldsymbol{x} = \begin{bmatrix} n_{\mathrm{u}a} \\ n_{\mathrm{l}a} \\ n_{\mathrm{u}b} \\ n_{\mathrm{l}b} \\ n_{\mathrm{u}c} \\ n_{\mathrm{l}c} \end{bmatrix}, \boldsymbol{b} = \begin{bmatrix} \alpha_1 i_{\mathrm{s}a}(k) \\ \alpha_1 i_{\mathrm{s}b}(k) \\ \alpha_1 i_{\mathrm{s}c}(k) \\ i_{\mathrm{z}a}(k) \\ i_{\mathrm{z}b}(k) \\ i_{\mathrm{z}c}(k) \end{bmatrix}$$

$$\boldsymbol{A} = \frac{T_{\mathrm{s}}}{3} \begin{bmatrix} \frac{-2\bar{v}_{\mathrm{u}a}}{L_{\mathrm{o}}} & \frac{2\bar{v}_{\mathrm{l}a}}{L_{\mathrm{o}}} & \frac{\bar{v}_{\mathrm{u}b}}{L_{\mathrm{o}}} & \frac{-\bar{v}_{\mathrm{l}b}}{L_{\mathrm{o}}} & \frac{\bar{v}_{\mathrm{u}c}}{L_{\mathrm{o}}} & \frac{-\bar{v}_{\mathrm{l}c}}{L_{\mathrm{o}}} \\ \frac{\bar{v}_{\mathrm{u}a}}{L_{\mathrm{o}}} & \frac{-\bar{v}_{\mathrm{l}a}}{L_{\mathrm{o}}} & \frac{-2\bar{v}_{\mathrm{u}b}}{L_{\mathrm{o}}} & \frac{2\bar{v}_{\mathrm{l}b}}{L_{\mathrm{o}}} & \frac{\bar{v}_{\mathrm{u}c}}{L_{\mathrm{o}}} & \frac{-\bar{v}_{\mathrm{l}c}}{L_{\mathrm{o}}} \\ \frac{\bar{v}_{\mathrm{u}a}}{L_{\mathrm{o}}} & \frac{-\bar{v}_{\mathrm{l}a}}{L_{\mathrm{o}}} & \frac{\bar{v}_{\mathrm{u}b}}{L_{\mathrm{o}}} & \frac{-\bar{v}_{\mathrm{l}b}}{L_{\mathrm{o}}} & \frac{-2\bar{v}_{\mathrm{u}c}}{L_{\mathrm{o}}} & \frac{2\bar{v}_{\mathrm{l}c}}{L_{\mathrm{o}}} \\ \frac{-\bar{v}_{\mathrm{u}a}}{L} & \frac{-\bar{v}_{\mathrm{l}a}}{L} & \frac{\bar{v}_{\mathrm{u}b}}{2L} & \frac{\bar{v}_{\mathrm{l}b}}{2L} & \frac{\bar{v}_{\mathrm{u}c}}{2L} & \frac{\bar{v}_{\mathrm{l}c}}{2L} \\ \frac{\bar{v}_{\mathrm{u}a}}{2L} & \frac{\bar{v}_{\mathrm{l}a}}{2L} & \frac{-\bar{v}_{\mathrm{u}b}}{L} & \frac{-\bar{v}_{\mathrm{l}b}}{L} & \frac{\bar{v}_{\mathrm{u}c}}{2L} & \frac{\bar{v}_{\mathrm{l}c}}{2L} \\ \frac{\bar{v}_{\mathrm{u}a}}{2L} & \frac{\bar{v}_{\mathrm{l}a}}{2L} & \frac{\bar{v}_{\mathrm{u}b}}{2L} & \frac{\bar{v}_{\mathrm{l}b}}{2L} & \frac{-\bar{v}_{\mathrm{u}c}}{L} & \frac{-\bar{v}_{\mathrm{l}c}}{L} \end{bmatrix}.$$

In (8), $\boldsymbol{y}$ presents the prediction values of ac-side currents and circulating currents at $k+1$ time instant and $\boldsymbol{x}$ is the vector of the insertion indices $n_{yx}$ ($y = u, l$ and $x = a, b, c$) for all six arms. $L_{\mathrm{o}} = 2L_{\mathrm{s}} + L$ is the ac-side equivalent inductance.

Assuming that the load is symmetric and thus the sum of the ac-side currents is zero. Based on the definition of the circulating current, the sum of the circulating currents is also equal to zero. Therefore, the Clarke transformation can be used to reduce the dimension of $\boldsymbol{y}$. The Clarke transformation is given by

$$\boldsymbol{C} = \frac{2}{3} \begin{bmatrix} 1 & -\frac{1}{2} & -\frac{1}{2} \\ 0 & \frac{\sqrt{3}}{2} & -\frac{\sqrt{3}}{2} \end{bmatrix}. \tag{9}$$

The augmented Clark matrix is defined as

$$\bar{\boldsymbol{C}} = \begin{bmatrix} \boldsymbol{C} & \boldsymbol{O}_{2\times 3} \\ \boldsymbol{O}_{2\times 3} & \boldsymbol{C} \end{bmatrix}. \tag{10}$$

The discrete-time mathematical model in the stationary $\alpha$-$\beta$ frame can be expressed as

$$\bar{\boldsymbol{y}} = \bar{\boldsymbol{A}}\boldsymbol{x} + \bar{\boldsymbol{b}} \tag{11}$$

where $\bar{\boldsymbol{y}} = \bar{\boldsymbol{C}}\boldsymbol{y}$, $\bar{\boldsymbol{A}} = \bar{\boldsymbol{C}}\boldsymbol{A}$, and $\bar{\boldsymbol{b}} = \bar{\boldsymbol{C}}\boldsymbol{b}$. Besides, $v_{\mathrm{sum}}$ and $v_{\mathrm{NO}}$ are used to control the dc-link current and eliminate the common-mode voltage, respectively. They are rewritten as

$$v_{\mathrm{sum}} = \underbrace{\frac{1}{3}\begin{bmatrix} \bar{v}_{\mathrm{u}a} & \bar{v}_{\mathrm{l}a} & \bar{v}_{\mathrm{u}b} & \bar{v}_{\mathrm{l}b} & \bar{v}_{\mathrm{u}c} & \bar{v}_{\mathrm{l}c} \end{bmatrix}}_{a_1}\boldsymbol{x}$$

$$v_{\mathrm{NO}} = \underbrace{\frac{1}{6}\begin{bmatrix} -\bar{v}_{\mathrm{u}a} & \bar{v}_{\mathrm{l}a} & -\bar{v}_{\mathrm{u}b} & \bar{v}_{\mathrm{l}b} & -\bar{v}_{\mathrm{u}c} & \bar{v}_{\mathrm{l}c} \end{bmatrix}}_{a_2}\boldsymbol{x}. \tag{12}$$

Finally, the augmented discrete-time mathematical model can be expressed as

$$\hat{\boldsymbol{y}} = \begin{bmatrix} i_{\mathrm{s}\alpha}(k+1) \\ i_{\mathrm{s}\beta}(k+1) \\ i_{\mathrm{z}\alpha}(k+1) \\ i_{\mathrm{z}\beta}(k+1) \\ i_{\mathrm{dc}}(k+1) \\ v_{\mathrm{NO}} \end{bmatrix} = \underbrace{\begin{bmatrix} \bar{\boldsymbol{A}} \\ -\frac{3T_{\mathrm{s}}}{2L}a_1 \\ a_2 \end{bmatrix}}_{\hat{\boldsymbol{A}}}\boldsymbol{x} + \underbrace{\begin{bmatrix} \bar{\boldsymbol{b}} \\ \frac{3T_{\mathrm{s}}}{2L}V_{\mathrm{dc}} \\ 0 \end{bmatrix}}_{\hat{\boldsymbol{b}}}. \tag{13}$$

Note that, (13) represents the model of the MMC system operating in the inverter mode. When the MMC system operates in the rectifier mode, $v_{\mathrm{sum}}$ should be directly controlled to the reference dc-link voltage $V_{\mathrm{dc}}^*$.

## III. Modulated MPC Algorithm for MMCs

The basic idea behind the modulated MPC of the MMC is to calculate the reference of insertion indices (or arm voltages) that can minimize the predefined cost function. By transforming the cost function into a QP problem about the control input $\boldsymbol{x}$ and solving this problem, we can easily obtain the reference values of the insertion index. The existing modulated methods introduced in [16], [19], [22] can be regarded as employing the unconstrained solution of this QP problem as the control input in this work, and they can be described as follows.

The cost function used in this work is defined in $\alpha$-$\beta$ frame as

$$\begin{aligned} J = {} & \left\|\boldsymbol{i}_{\mathrm{s}\alpha\beta}^* - \boldsymbol{i}_{\mathrm{s}\alpha\beta}(k+1)\right\|_2^2 + w_1\left\|\boldsymbol{i}_{\mathrm{z}\alpha\beta}^* - \boldsymbol{i}_{\mathrm{z}\alpha\beta}(k+1)\right\|_2^2 \\ & + w_2\left\|i_{\mathrm{dc}}^* - i_{\mathrm{dc}}(k+1)\right\|_2^2 + w_3\left\|v_{\mathrm{NO}}^* - v_{\mathrm{NO}}\right\|_2^2 \end{aligned} \tag{14}$$

where $\|\cdot\|_2^2$ is the squared 2-norm. $w_1$, $w_2$, and $w_3$ are weighting factors of circulating currents, dc-link current, and common-mode voltage, respectively. Note that the selection of the weighting factor is an open issue in academia. However, we can adjust these weighting factors in a trial-and-error manner until satisfactory control performance is achieved. The way to obtain the reference value of circulating currents can be found in [5], [24].

The cost function in (14) can be written as a standard QP problem about $\boldsymbol{x} = [n_{\mathrm{u}a}\, n_{\mathrm{l}a}\, n_{\mathrm{u}b}\, n_{\mathrm{l}b}\, n_{\mathrm{u}c}\, n_{\mathrm{l}c}]^{\mathrm{T}}$ as

$$\begin{aligned} & \min_{\boldsymbol{x}} J(\boldsymbol{x}) = \frac{1}{2}\boldsymbol{x}^{\mathrm{T}}\boldsymbol{Q}\boldsymbol{x} + \boldsymbol{d}^{\mathrm{T}}\boldsymbol{x} \\ & \text{subject to } \boldsymbol{0} \preceq \boldsymbol{x} \preceq N \end{aligned} \tag{15}$$

where $\boldsymbol{Q} = \hat{\boldsymbol{A}}^{\mathrm{T}}\boldsymbol{W}\hat{\boldsymbol{A}}$, and $\boldsymbol{d} = \hat{\boldsymbol{A}}^{\mathrm{T}}\boldsymbol{W}(\hat{\boldsymbol{b}} - \boldsymbol{y}^*)$, with diagonal weighting matrix $\boldsymbol{W} = \mathrm{diag}(1, 1, w_1, w_1, w_2, w_3)$, $\boldsymbol{y}^* = [i_{\mathrm{s}\alpha}^*\, i_{\mathrm{s}\beta}^*\, i_{\mathrm{z}\alpha}^*\, i_{\mathrm{z}\beta}^*\, i_{\mathrm{dc}}^*\, v_{\mathrm{NO}}^*]^{\mathrm{T}}$, $\boldsymbol{0} = [0\,0\,0\,0\,0\,0]^{\mathrm{T}}$, and $\boldsymbol{N} = [N\,N\,N\,N\,N\,N]^{\mathrm{T}}$.

It should be noted that in this case the insertion indices defined in $\boldsymbol{x}$ are selected as control variables. The arm voltage ($\boldsymbol{v} = [v_{\mathrm{u}a}\, v_{\mathrm{l}a}\, v_{\mathrm{u}b}\, v_{\mathrm{l}b}\, v_{\mathrm{u}c}\, v_{\mathrm{l}c}]^{\mathrm{T}}$) can also be used as the control variable [16], [22]. $\boldsymbol{v}$ is the vector of all arm voltages of the three phases. The relationship between these two types of control

variables ($\boldsymbol{x}$ and $\boldsymbol{v}$) is expressed as follows:

$$\boldsymbol{v} = \bar{\boldsymbol{V}}\boldsymbol{x} \tag{16}$$

where $\bar{\boldsymbol{V}} = \mathrm{diag}(\bar{v}_{\mathrm{ua}}, \bar{v}_{\mathrm{la}}, \bar{v}_{\mathrm{ub}}, \bar{v}_{\mathrm{lb}}, \bar{v}_{\mathrm{uc}}, \bar{v}_{\mathrm{lc}})$. The two modeling method with different control variables are essentially equivalent. The unconstrained solution of (15) can be expressed as

$$\boldsymbol{x}_{\mathrm{unc}} = -\boldsymbol{Q}^{-1}\boldsymbol{d} = \hat{\boldsymbol{A}}^{-1}(\boldsymbol{y}^* - \hat{\boldsymbol{b}}) \tag{17}$$

and the desired arm voltage can be obtained by $\boldsymbol{v}_{\mathrm{unc}} = \bar{\boldsymbol{V}}\boldsymbol{x}_{\mathrm{unc}}$ [16]. We can find that the unconstrained solution (17) derived from our designed cost function has the same solution form as the deadbeat control. It is worth noting that not all unconstrained solutions derived from the cost function have the same form as the deadbeat control solution. But in our designed cost function, they are equivalent.

### A. Limitations of the Existing Modulated MPC for MMCs

As the method introduced in [18] has been fully discussed in [22], this section will mainly focus on another class of modulated MPC schemes [16], [19], [22]. This part will reveal the main idea behind these methods and their limitations.

To better illustrate the idea of these methods, the per-phase model has been used [19], [22] and it can be expressed as

$$\underbrace{\begin{bmatrix} i_{sx}(k+1) \\ i_{\mathrm{cir}x}(k+1) \end{bmatrix}}_{\boldsymbol{y}} = \underbrace{\begin{bmatrix} -\frac{T_s}{L_o} & \frac{T_s}{L_o} \\ -\frac{T_s}{2L} & -\frac{T_s}{2L} \end{bmatrix}}_{\boldsymbol{B}} \underbrace{\begin{bmatrix} v_{ux}(k) \\ v_{lx}(k) \end{bmatrix}}_{\boldsymbol{u}} + \underbrace{\begin{bmatrix} \left(1 - \frac{2R_sT_s}{L_o}\right) i_{sx}(k) \\ i_{\mathrm{cir}x}(k) + \frac{T_s}{2L}V_{\mathrm{dc}}(k) \end{bmatrix}}_{\boldsymbol{d}} \tag{18}$$

where $i_{\mathrm{cir}x} = i_{zx} + i_{\mathrm{dc}}/3$ and $x = a, b, c$. The cost function for the per-phase model is designed as

$$J(\boldsymbol{u}) = (\boldsymbol{y}^* - \boldsymbol{y})^{\mathrm{T}}\boldsymbol{W}(\boldsymbol{y}^* - \boldsymbol{y}) \tag{19}$$

where $\boldsymbol{y}^* = \begin{bmatrix} i_{sx}^* & i_{\mathrm{cir}x}^* \end{bmatrix}^{\mathrm{T}}$ and $\boldsymbol{W} = \mathrm{diag}(1, w_1)$. $\boldsymbol{u}$ is the control input in the per-phase model, which represents the upper and lower arm voltages of phase $x$. Applying (18) into (19) and neglecting the constant term in $J(\boldsymbol{u})$, the cost function can be rewritten as

$$\tilde{J}(\boldsymbol{u}) = \boldsymbol{u}^{\mathrm{T}}\boldsymbol{B}^{\mathrm{T}}\boldsymbol{W}\boldsymbol{B}\boldsymbol{u} + 2(\boldsymbol{d} - \boldsymbol{y}^*)^{\mathrm{T}}\boldsymbol{W}\boldsymbol{B}\boldsymbol{u}. \tag{20}$$

The unconstrained solution of (20) can be derived as

$$\boldsymbol{u}_{\mathrm{unc}} = (\boldsymbol{B}^{\mathrm{T}}\boldsymbol{W}\boldsymbol{B})^{-1}\Big((\boldsymbol{y}^* - \boldsymbol{d})^{\mathrm{T}}\boldsymbol{W}\boldsymbol{B}\Big)^{\mathrm{T}} = \boldsymbol{B}^{-1}(\boldsymbol{y}^* - \boldsymbol{d}). \tag{21}$$

The similar expression can be found in [19].

*Remark 1:* Note that although the different models has been utilized, the solutions obtained by these methods [16], [19], [22] will be the same as long as the reference value of the common-mode voltage is set to 0 and $i_{\mathrm{cir}x}^* = i_{zx}^* + i_{\mathrm{dc}}^*/3$. However, in practice, when the common-mode voltage is not 0, the predicted value obtained by using the three-phase model will be more accurate. Thus, in the experimental part, the method in [16] will be used to compare with our method.

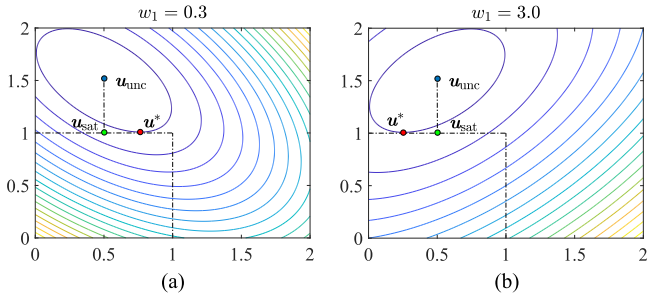


Fig. 2. Optimal solutions with different $w_1$. (a) $w_1 = 0.3$. (b) $w_1 = 3.0$.

From (21), it seems that the weighting factor is not required. However, this solution ignores the actual physical constraints of the system. The control input $\boldsymbol{u}$ should naturally satisfy the following constraints:

$$0 \le v_{ux}(k) \le \sum_{i=1}^{N} v_{\mathrm{c},ux}^i,\ 0 \le v_{lx}(k) \le \sum_{i=1}^{N} v_{\mathrm{c},lx}^i. \tag{22}$$

When the solution obtained by (21) does not satisfy these constraints (22), the common measure [25] is to saturate this solution, which can be expressed as

$$\boldsymbol{u}_{\mathrm{sat}} = \min(\boldsymbol{u}_{\mathrm{b}}, \max(\boldsymbol{l}_{\mathrm{b}}, \boldsymbol{u}_{\mathrm{unc}})). \tag{23}$$

$\boldsymbol{l}_{\mathrm{b}} = [0\,0]^{\mathrm{T}}$ and $\boldsymbol{u}_{\mathrm{b}} = \begin{bmatrix} \sum_{i=1}^{N} v_{\mathrm{c},ux}^i & \sum_{i=1}^{N} v_{\mathrm{c},lx}^i \end{bmatrix}^{\mathrm{T}}$ represent the lower bound and upper bound of the control variable $\boldsymbol{u}$, respectively. This saturation approach is proper when $\boldsymbol{B}^{\mathrm{T}}\boldsymbol{W}\boldsymbol{B}$ is a positive semidefinite diagonal matrix, which is common in decoupled control. However, such a saturation manner cannot get the optimal solution in most cases and, thus, the effect of the weighting factor is highlighted. To better illustrate the effect of different weighting factors on the optimal solution, a simple example has been given as follows:

$$\boldsymbol{B} = \begin{bmatrix} 1 & 1 \\ -1 & 1 \end{bmatrix}, \boldsymbol{d} - \boldsymbol{y}^* = \begin{bmatrix} -2 \\ -1 \end{bmatrix}, \boldsymbol{l}_b = \begin{bmatrix} 0 \\ 0 \end{bmatrix}, \boldsymbol{u}_b = \begin{bmatrix} 1 \\ 1 \end{bmatrix}. \tag{24}$$

According to (21), the unconstrained solution can be easily obtained: $\boldsymbol{u}_{\mathrm{unc}} = \begin{bmatrix} 0.5 & 1.5 \end{bmatrix}^{\mathrm{T}}$. We can obtain different optimal solutions when the weighting factor $w_1$ is different. Fig. 2 is a contour plot of the cost function $\tilde{J}$ (the $x$-axis and $y$-axis of Fig. 2 are the two elements of the control input $\boldsymbol{u}$). It describes the different location of the optimal solution when $w_1$ is equal to 0.3 and 3.0, respectively. It can be seen that the unconstrained solutions $\boldsymbol{u}_{\mathrm{unc}}$ and the corresponding saturation solutions $\boldsymbol{u}_{\mathrm{sat}}$ are the same for two weighting factors. However, the optimal solutions $\boldsymbol{u}^*$ in Fig. 2(a) and (b) are different due to the different weighting factors. Obviously, applying different optimal solutions will result in different control performance. Therefore, well-designed weighting factors that consider the importance

of different control objectives will bring a satisfactory control performance for the system. Instead, by using the saturation solution, the control performance is independent of the weights, which also means that the control performance of the most important control objective cannot be guaranteed. This is the limitation of the existing modulated MPC methods. Fig. 2(a) and (b) also reveals that the control input $\boldsymbol{u}_{\text{sat}}$ closest to the unconstrained solution $\boldsymbol{u}_{\text{unc}}$ cannot bring the control objectives closest to their reference values. Therefore, for the modulated MPC scheme, the effect of the weighting factor cannot be ignored when the unconstrained solution is not in the feasible region (this situation usually occurs when the system is in a high modulation index or transients).

### B. Proposed Modulated MPC Algorithm for MMCs

As discussed in the previous section, using the unconstrained solution will deteriorate the control performance in some cases and thus it is necessary to employ the optimal solution to the control system. The proposed modulated MPC scheme adopts a bound-constrained QP method to quickly obtain the optimal solution of the problem (15).

Corresponding to the constrained optimization problem (15), one can form a Lagrangian function as

$$\mathcal{L}(\boldsymbol{x},\boldsymbol{s},\boldsymbol{t}) = \frac{1}{2}\boldsymbol{x}^{\mathrm{T}}\boldsymbol{Q}\boldsymbol{x} + \boldsymbol{d}^{\mathrm{T}}\boldsymbol{x} + \boldsymbol{s}^{\mathrm{T}}(\boldsymbol{x}-\boldsymbol{N}) + \boldsymbol{t}^{\mathrm{T}}(\boldsymbol{0}-\boldsymbol{x}) \tag{25}$$

where $\boldsymbol{s}$ and $\boldsymbol{t}$ are Lagrange multipliers. The Karush–Kuhn–Tucker (KKT) condition [26] is given by

$$\boldsymbol{Q}\boldsymbol{x} + \boldsymbol{d} + \boldsymbol{s} - \boldsymbol{t} = \boldsymbol{0} \tag{26a}$$

$$s_i(x_i - N) = 0, \forall i \in \mathcal{C} \tag{26b}$$

$$t_i(0 - x_i) = 0, \forall i \in \mathcal{C} \tag{26c}$$

$$\boldsymbol{0} \preceq \boldsymbol{x} \preceq \boldsymbol{N}, \boldsymbol{s} \succeq \boldsymbol{0}, \boldsymbol{t} \succeq \boldsymbol{0} \tag{26d}$$

where $\mathcal{C} = \{1, 2, \ldots, n\}$, $n$ is the dimension of $\boldsymbol{x}$. It is well known that the QP problem (15) reaches the minimum if and only if $(\boldsymbol{x}, \boldsymbol{s}, \boldsymbol{t})$ satisfies the KKT conditions in (26). The crucial point in solving (15) is to identify those inequalities that are active. Besides, in practical applications, the speed of finding these active constraints is also important. An infeasible active set method [23] for solving such a QP problem is adopted due to its fast convergence. This method only requires very few iterations to solve a QP problem. To describe the algorithm briefly, some working sets ($\mathcal{A}_l$, $\mathcal{A}_u$, and $\mathcal{I}$) are declared in advance. $\mathcal{A}_l$ is the index set for which the lower bound constraint is active. For each $i \in \mathcal{A}_l$, $x_i$ will touch the lower bound, which is $x_i = 0$ in this case. Similarly, $\mathcal{A}_u$ is the index set for which the upper bound constraint is active. For each $i \in \mathcal{A}_u$, there is $x_i = N$. $\mathcal{A}$ is the set for active constraints and it can be expressed as $\mathcal{A} = \mathcal{A}_l \cup \mathcal{A}_u$. Set $\mathcal{I}$ is the complementary set of $\mathcal{A}$ and it can be obtained by $\mathcal{I} = \mathcal{C} \setminus \mathcal{A}$. It assumes that for each $i \in \mathcal{I}$, $x_i$ neither exceeds the lower nor the upper bound. According to the present working sets ($\mathcal{A}_u$, $\mathcal{A}_l$, and $\mathcal{I}$) and KKT conditions (26b) and (26c), we can easily obtain the following equations as:

$$\begin{aligned} \boldsymbol{x}_{\mathcal{A}_l} &= \boldsymbol{0},\ \boldsymbol{s}_{\mathcal{A}_l} = \boldsymbol{0} \\ \boldsymbol{x}_{\mathcal{A}_u} &= \boldsymbol{N},\ \boldsymbol{t}_{\mathcal{A}_u} = \boldsymbol{0} \\ \boldsymbol{s}_{\mathcal{I}} &= \boldsymbol{0},\ \boldsymbol{t}_{\mathcal{I}} = \boldsymbol{0}. \end{aligned} \tag{27}$$

Now only $\boldsymbol{x}_{\mathcal{I}}$, $\boldsymbol{s}_{\mathcal{A}_u}$, and $\boldsymbol{t}_{\mathcal{A}_l}$ need to be solved. According to (26a), these variables can be obtained by solving the following equation as:

$$\begin{bmatrix} \boldsymbol{Q}_{\mathcal{A}_u\mathcal{A}_u} & \boldsymbol{Q}_{\mathcal{A}_u\mathcal{A}_l} & \boldsymbol{Q}_{\mathcal{A}_u\mathcal{I}} \\ \boldsymbol{Q}_{\mathcal{A}_l\mathcal{A}_u} & \boldsymbol{Q}_{\mathcal{A}_l\mathcal{A}_l} & \boldsymbol{Q}_{\mathcal{A}_l\mathcal{I}} \\ \boldsymbol{Q}_{\mathcal{I}_I\mathcal{A}_u} & \boldsymbol{Q}_{\mathcal{I}_I\mathcal{A}_l} & \boldsymbol{Q}_{\mathcal{I}\mathcal{I}} \end{bmatrix} \begin{bmatrix} \boldsymbol{x}_{\mathcal{A}_u} \\ \boldsymbol{x}_{\mathcal{A}_l} \\ \boldsymbol{x}_{\mathcal{I}} \end{bmatrix} + \begin{bmatrix} \boldsymbol{d}_{\mathcal{A}_u} \\ \boldsymbol{d}_{\mathcal{A}_l} \\ \boldsymbol{d}_{\mathcal{I}} \end{bmatrix} + \begin{bmatrix} \boldsymbol{s}_{\mathcal{A}_u} \\ \boldsymbol{s}_{\mathcal{A}_l} \\ \boldsymbol{s}_{\mathcal{I}} \end{bmatrix} - \begin{bmatrix} \boldsymbol{t}_{\mathcal{A}_u} \\ \boldsymbol{t}_{\mathcal{A}_l} \\ \boldsymbol{t}_{\mathcal{I}} \end{bmatrix} = \boldsymbol{0}. \tag{28}$$

Based on (27), $\boldsymbol{x}_{\mathcal{I}}$ can be solved first by

$$\boldsymbol{Q}_{\mathcal{I}\mathcal{I}}\boldsymbol{x}_{\mathcal{I}} = -\boldsymbol{d}_{\mathcal{I}} - \boldsymbol{Q}_{\mathcal{I}\mathcal{A}_u}\boldsymbol{x}_{\mathcal{A}_u} - \boldsymbol{Q}_{\mathcal{I}\mathcal{A}_l}\boldsymbol{x}_{\mathcal{A}_l} \tag{29}$$

where $\boldsymbol{Q}_{\mathcal{I}\mathcal{I}}$ is convex and, hence, the system (29) is solvable. After $\boldsymbol{x}_{\mathcal{I}}$ is solved, the $\boldsymbol{s}_{\mathcal{A}_u}$ and $\boldsymbol{t}_{\mathcal{A}_l}$ can be obtained as

$$\begin{aligned} \boldsymbol{s}_{\mathcal{A}_u} &= -\boldsymbol{Q}_{\mathcal{A}_u\mathcal{A}_u}\boldsymbol{x}_{\mathcal{A}_u} - \boldsymbol{Q}_{\mathcal{A}_u\mathcal{A}_l}\boldsymbol{x}_{\mathcal{A}_l} - \boldsymbol{Q}_{\mathcal{A}_u\mathcal{I}}\boldsymbol{x}_{\mathcal{I}} - \boldsymbol{d}_{\mathcal{A}_u} \\ \boldsymbol{t}_{\mathcal{A}_l} &= \boldsymbol{Q}_{\mathcal{A}_l\mathcal{A}_u}\boldsymbol{x}_{\mathcal{A}_u} + \boldsymbol{Q}_{\mathcal{A}_l\mathcal{A}_l}\boldsymbol{x}_{\mathcal{A}_l} + \boldsymbol{Q}_{\mathcal{A}_l\mathcal{I}}\boldsymbol{x}_{\mathcal{I}} + \boldsymbol{d}_{\mathcal{A}_l}. \end{aligned} \tag{30}$$

All the variables have been solved based on the present active set $\mathcal{A}$. If our guess for the present active set $\mathcal{A}$ is correct, then $\boldsymbol{0} \preceq \boldsymbol{x}_{\mathcal{I}} \preceq \boldsymbol{N}$, $\boldsymbol{s}_{\mathcal{A}_u} \succeq \boldsymbol{0}$, and $\boldsymbol{t}_{\mathcal{A}_l} \succeq \boldsymbol{0}$ will be satisfied. Otherwise, a new guess for the working sets $\mathcal{A}_l$, $\mathcal{A}_u$, and $\mathcal{A}$ should be made for the next iteration, which we denote by $\mathcal{A}_l^+$, $\mathcal{A}_u^+$, and $\mathcal{A}^+$. Consider the following cases. If $s_i > 0$ ($i \in \mathcal{A}_u$), it indicates that our previous guess $i \in \mathcal{A}_u$ is reasonable. Similarly, if $t_i > 0$ ($i \in \mathcal{A}_l$), the index of $t_i$ should be included in the new working set $\mathcal{A}_l^+$. $\boldsymbol{x}_{\mathcal{I}}$ should also be checked and, thus, the guess for the new working sets can be summarized as follows:

$$\begin{aligned} \mathcal{A}_l^+ &= \{i : x_i < 0, \text{or}\, x_i = 0\,\&\, t_i > 0\} \\ \mathcal{A}_u^+ &= \{i : x_i > N, \text{or}\, x_i = N\,\&\, s_i > 0\} \\ \mathcal{A}^+ &= \mathcal{A}_l^+ \cup \mathcal{A}_u^+ \quad . \end{aligned} \tag{31}$$

With these new working sets, we can repeat the procedure to get the new solution and check whether the KKT condition is satisfied. The detail of convergence analysis of the algorithm can be found in [23]. An intuitive description about this algorithm are summarized in Algorithm 1.

*Remark 2:* It should be noted that the main computational burden of this method is matrix inversion for $\boldsymbol{Q}$. Due to the relatively small scale of the problem (six dimensions) and the low number of iterations required to solve the problem, all calculations can be completed within one control cycle. To further reduce the calculation load, the arm voltage should be used as the control variables. In this way, the matrix $\boldsymbol{Q}$ is constant and its inverse matrix can be calculated offline and stored in advance. In fact, since the inverse matrix is known, we can go through all possible active sets to find the solution for the optimization problem. The calculation time may increase, but

**Algorithm 1:** Infeasible Active-Set Method.

**function** IAS($\boldsymbol{Q}, \boldsymbol{d}, \boldsymbol{a}, \boldsymbol{b}$)
  $\mathcal{C} \leftarrow \{1, 2, \ldots, n\}$
  $\mathcal{A}_u \leftarrow \emptyset, \mathcal{A}_l \leftarrow \emptyset, \mathcal{I} \leftarrow \mathcal{C} \setminus \mathcal{A}_u \setminus \mathcal{A}_l$
  Flag $\leftarrow 0$
  **while** Flag $== 0$ **do**
    $\boldsymbol{x}_{\mathcal{A}_u} \leftarrow \boldsymbol{b}_{\mathcal{A}_u}$ {$\boldsymbol{b}$ is the upper bound}
    $\boldsymbol{x}_{\mathcal{A}_l} \leftarrow \boldsymbol{a}_{\mathcal{A}_l}$ {$\boldsymbol{a}$ is the lower bound}
    $\boldsymbol{s}_{\mathcal{I}\cup\mathcal{A}_l} \leftarrow \boldsymbol{0}$
    $\boldsymbol{t}_{\mathcal{I}\cup\mathcal{A}_u} \leftarrow \boldsymbol{0}$
    Compute $(\boldsymbol{x}_{\mathcal{I}}, s_{\mathcal{A}_u}, t_{\mathcal{A}_l})$ from (29) and (30)
    **if** $\boldsymbol{a} \preceq \boldsymbol{x} \preceq \boldsymbol{b}$ & $\boldsymbol{s} \succeq 0$ & $\boldsymbol{t} \succeq 0$ **then**
      $\boldsymbol{x}^* = \boldsymbol{x}$
      Flag $\leftarrow 1$
    **end if**
    $\mathcal{A}_u = \mathcal{A}_u^+ \leftarrow \{i : x_i > b_i \parallel s_i > 0\}$
    $\mathcal{A}_l = \mathcal{A}_l^+ \leftarrow \{i : x_i < a_i \parallel t_i > 0\}$
    $\mathcal{I} = \mathcal{I}^+ \leftarrow \mathcal{C} \setminus \mathcal{A}_u^+ \setminus \mathcal{A}_l^+$
  **end while**
  **return** $\boldsymbol{x}^*$
**end function**

for some ill-conditioned cases, this manner guarantees that the optimal solution will definitely be found in a determined time.

So far, after implementing this infeasible active set method, the optimal solution $\boldsymbol{x}^*$, which presents the insertion index of each arm, can be obtained. This solution can be directly applied to the sorting and modulation stage to realize the control of the MMC system.

### C. Voltage Balancing and Modulation Method

The arm-balancing control can be used to stabilize the MMC operation and generate the reference of the circulating current [24]. The individual balancing of each SM is based on the sorting algorithm. However, the insertion indices obtained by the modulated MPC scheme are not integer and, thus, some modifications have to be made before implementing the sorting algorithm.

According to the optimal solution $\boldsymbol{x}^*$, the number of SMs that remain inserted during one control period can be expressed as

$$n_{yx}^{\inf} = \text{floor}(n_{yx}^*) \tag{32}$$

where $n_{yx}^*$ is the element of $\boldsymbol{x}^*$ and the floor function will generate the greatest integer $n_{yx}^{\inf}$, which is less than or equal to $n_{yx}^*$. The fractional part of $n_{yx}^*$, which represents the duty cycle of the SM operating under the PWM mode, can be calculated as

$$d_{yx} = n_{yx}^* - n_{yx}^{\inf}. \tag{33}$$

The maximum number of inserted SMs in a control period can be expressed as

$$n_{yx}^{\sup} = \text{ceil}(n_{yx}^*). \tag{34}$$

The ceiling function maps $n_{yx}^*$ to the least integer greater than or equal $n_{yx}^*$. $n_{yx}^{\sup}$ will be given to the voltage sorting algorithm to determine which SMs need to be inserted. $n_{yx}^{\inf}$ SMs will be inserted during the whole control period and the duty cycles of these SMs will be given as 1. $N - n_{yx}^{\sup}$ SMs will be bypassed during the whole control period and the duty cycles of these SMs will be given as 0. The state of an SM will change according to the corresponding duty cycle $d_{yx}$. When the duty cycle of all SMs is obtained, each SM will complete the modulation process according to its own duty cycle. Fig. 3 shows the block diagram of the voltage sorting part and modulation part.

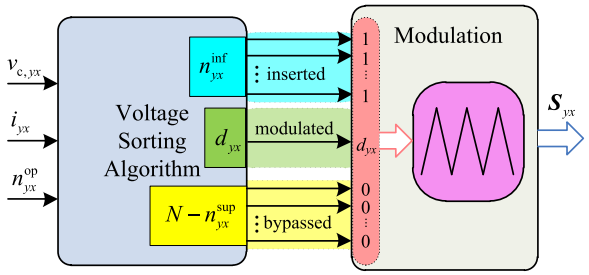


Fig. 3. Block diagram of voltage balancing algorithm and modulation method.

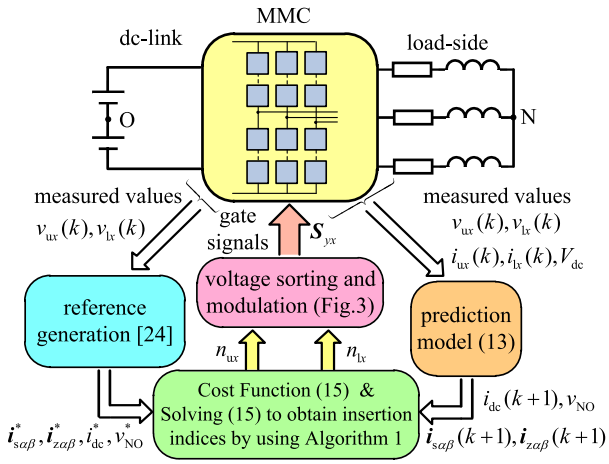


Fig. 4. Block diagram of the proposed modulated MPC scheme.

### D. Control Structure of the Proposed Modulated MPC

The overall control block diagram of the proposed modulated MPC method is presented in Fig. 4. According to the designed cost function (14), four control objectives, i.e., ac-side currents $\boldsymbol{i}_{\text{s}}$, circulating currents $\boldsymbol{i}_{\text{z}}$, dc-link current $i_{\text{dc}}$, and the common-mode voltage $v_{\text{NO}}$, should be controlled at the same time in the predictive controller. It is worth noting that the reference of the circulating current is achieved by using an external voltage balancing method. When MMC operates at nominal frequency, the balancing method introduced in [24] will be adopted, while when MMC operates at low frequencies, we will employ the high-frequency circulating current injection method from [5]. At first, the MPC scheme uses the discrete-time model (7), which is also called prediction model, to obtain the predicted values of the control variables at $k+1$ time instant. Note that, these predicted values are related to the insertion indices $\boldsymbol{x}$. The problem now is how to solve for $\boldsymbol{x}$. By using Algorithm 1, the reference of

TABLE I
PARAMETERS FOR THE EXPERIMENTAL PLATFORM

| Parameter | Symbol | Value |
|---|---|---|
| DC-link voltage | $V_{\mathrm{dc}}$ | 100 V |
| Number of SMs per Arm | $N$ | 2 |
| SM Capacitance | $C_{\mathrm{SM}}$ | 5.04 mF |
| Arm Inductance | $L$ | 1.9 mH |
| AC-side Resistance | $R_{\mathrm{s}}$ | 5 Ω |
| AC-side Inductance | $L_{\mathrm{s}}$ | 6.8 mH |

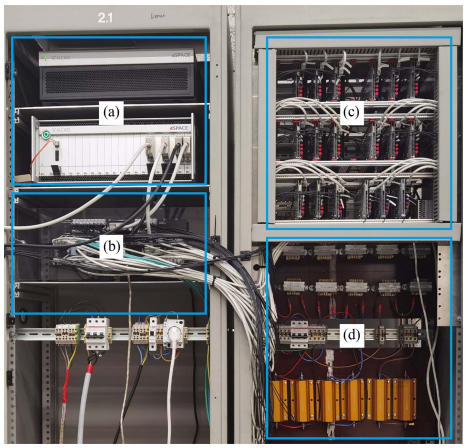


Fig. 5. Setup of the testbench. (a) dSPACE SCALEXIO real-time system. (b) Interface. (c) Three phase MMC. (d) RL load.

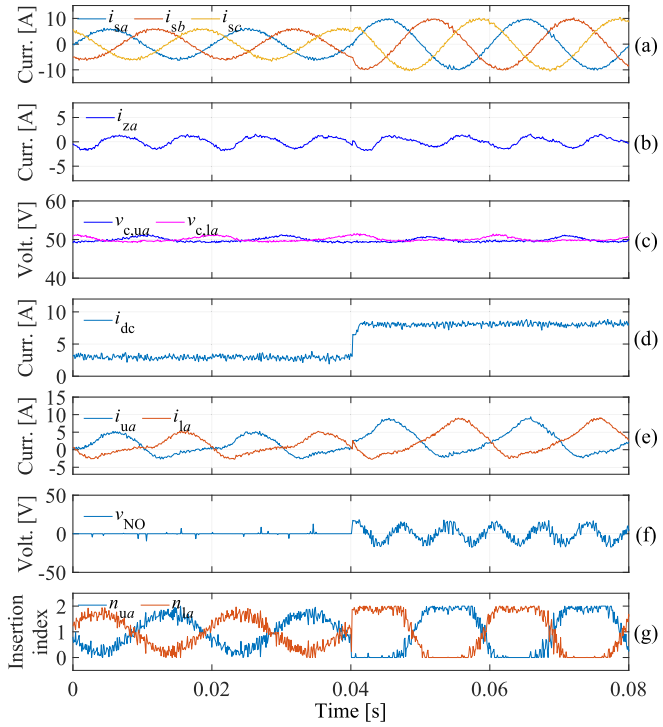


Fig. 6. Step change in AC currents with the proposed MPC at 50 Hz. (a) ac-side currents. (b) circulating current of phase a. (c) SM capacitor voltages of the upper and lower arms. (d) dc-link current. (e) upper and lower arm currents of phase a. (f) common-mode voltage. (g) insertion indices of the upper and lower arms.

the insertion indices, which minimizes the cost function (14) or the QP problem (15), can be obtained. After that, these reference values are sent to the sorting and modulation part shown in Fig. 3 and converted into switching signals to the MMC.

## IV. VALIDATIONS

The parameters of the MMC system with $RL$ load have been given in Table I and the photo of the test bench is shown in Fig. 5. The sampling interval is 100 µs. In this section, the experimental results of both the conventional modulated MPC methods [16], [18] and the proposed method will be presented.

### A. MMC Operates at High Modulation Index and Transients

To verify the effectiveness of the proposed modulated MPC method, we conducted a comparative study between the proposed method and the existing conventional modulated MPC methods [16], [18]. For the sake of distinction, we refer to the method introduced in [16] as conventional MPC 1. As discussed in Section III, conventional MPC 1 does not consider the constraints of the control input, which is the only difference from the proposed method in this work. The control method in [18] is called conventional MPC 2 in this part.

The experimental results of the proposed method under the step change in the output currents (from 6 to 10A) are shown in Fig. 6. The weighting factors used in the proposed method are $w_{\mathrm{o}} = 1, w_1 = 0.3, w_2 = 0.3, w_3 = 1 \times 10^{-6}$. $w_{\mathrm{o}}$ is the weighting factor for ac-side currents. Note that the conventional MPC methods do not require weighting factors. Fig. 6(a) presents the three-phase ac-side currents ($i_{sa}$, $i_{sb}$, and $i_{sc}$) at such a related change. Fig. 6(b) shows the circulating current of phase $a$ ($i_{za}$). As the low-pass/notch filters are not applied in the energy control part, a second-order component appears in the circulating current. The capacitor voltages of the upper and lower arm in leg $a$ ($v_{\mathrm{c},ua}$ and $v_{\mathrm{c},la}$) is shown in Fig. 6(c). It can be seen that the SM capacitor voltages in both the upper and lower arms are well balanced. Fig. 6(d) and (e) shows the dc-link current ($i_{\mathrm{dc}}$) and the upper and lower arm currents ($i_{ua}$ and $i_{la}$). Fig. 6(f) represents the equivalent common-mode voltage over one control period ($v_{\mathrm{NO}}$). The insertion index waveforms of the upper and lower arms are also provided in Fig. 6(g).

The control performance of the conventional MPC 1 has been provided in Fig. 7 . To show more details, we have also provided detailed waveforms of the output current and dc-link current during a step change in the output current reference, as shown in Fig. 11. It can be seen that a comparable steady-state performance can be achieved when the amplitude of the ac-side currents is 6 A. However, poor dynamic response is observed in the dc-link current. Besides, there are obvious fluctuations in the dc-link current when the amplitude of the ac-side currents is 10 A. In fact, we can find from Fig. 11 that there is a steady-state error on the dc-link current with conventional MPC 1. This is why the settling time of its dc-link current is infinite, as shown in Table II. We can also observe from Figs. 10–12 that the dynamic responses of the output currents are similar among these three methods. However, while conventional MPC 1 ensures the control performance of the output current, it fails to address other control objectives, such as the dc-link current. Comparing Figs. 6

TABLE II
COMPARISON OF OVERALL PERFORMANCE AMONG THREE METHODS

| | Proposed MPC | Conventional MPC 1 | Conventional MPC 2 |
|---|---|---|---|
| THD of output current (6 A/10 A) | 3.66%/2.21% | 3.83%/2.86% | 3.68%/3.27% |
| RMS of circulating current (6 A/10 A) | 0.97 A/0.87 A | 0.97 A/1.08 A | 0.95 A/0.83 A |
| Calculation time | 17.8 μs (7 iterations) | 17.3 μs (1 iteration) | 18.4 μs (9 cycles) |
| Rise time of output current | 1 ms | 0.9 ms | 1.1 ms |
| Rise time of dc-link current | 1.2 ms | inf | 1.3 ms |

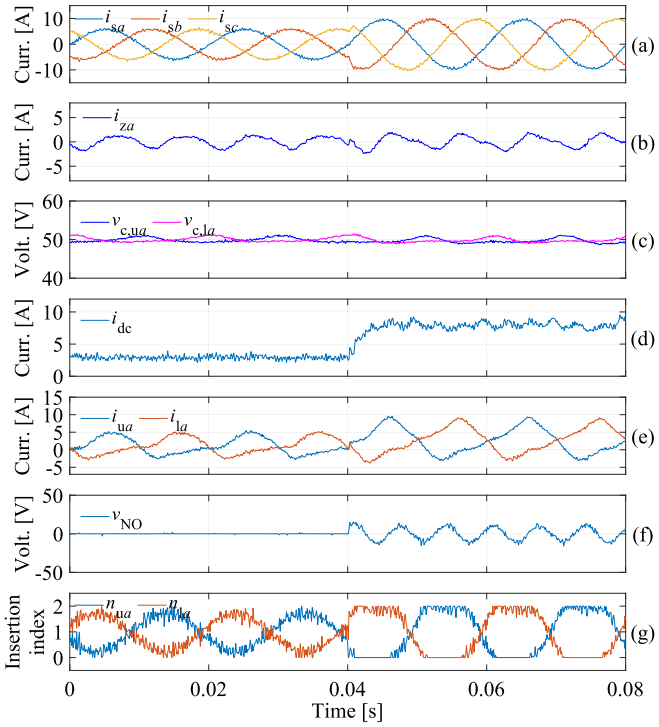


Fig. 7. Step change in AC currents with conventional MPC 1 at 50 Hz. (a) ac-side currents. (b) circulating current of phase a. (c) SM capacitor voltages of the upper and lower arms. (d) dc-link current. (e) upper and lower arm currents of phase a. (f) common-mode voltage. (g) insertion indices of the upper and lower arms.

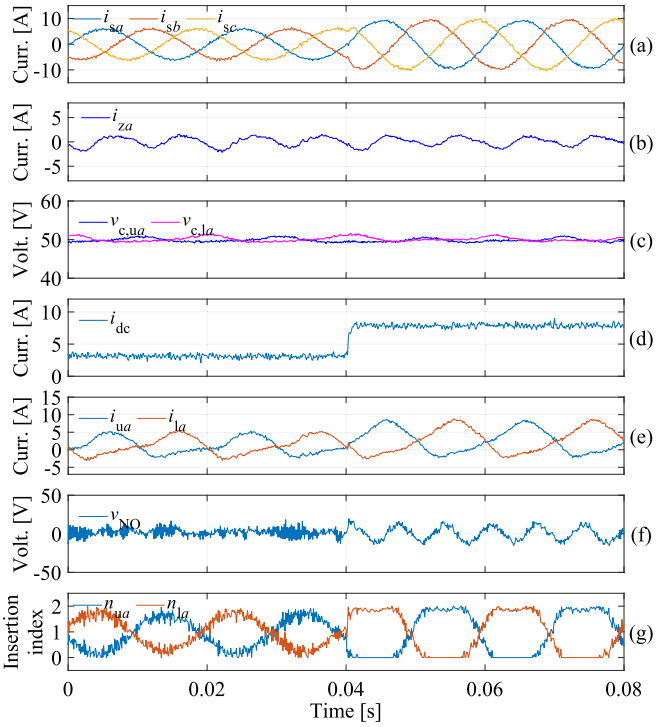


Fig. 8. Step change in AC currents with conventional MPC 2 at 50 Hz. (a) ac-side currents. (b) circulating current of phase a. (c) SM capacitor voltages of the upper and lower arms. (d) dc-link current. (e) upper and lower arm currents of phase a. (f) common-mode voltage. (g) insertion indices of the upper and lower arms.

and 10 with Figs. 7 and 11, we can observe that both the dynamic response and steady-state performance of the dc-link current show that the proposed modulated MPC method outperforms the conventional MPC 1, which validates the analysis in Section III-A. To evaluate the control performance of the circulating current, the root-mean-square (RMS) values are also provided in Table II. We can conclude similarly that, when the output current is 6 A, the RMS value of the circulating current for the proposed method and conventional MPC 1 is almost the same. However, when the output current increases to 10 A, the RMS value of the circulating current of the conventional method is slightly larger than that of the proposed method. The conventional MPC 2 also provides satisfactory control performance in the case of MMC operating at a low modulation index, which is shown in Fig. 8. It can be seen from Fig. 8(b) that the dynamic response of the circulating current with conventional MPC 2 is faster than the other two methods. In addition, the steady-state performance of the dc-link current (dc) and the circulating current with this method is superior to that of conventional MPC 1 at high modulation index. However, when the MMC is operating at a high modulation index, the three-phase currents exhibit significant distortions shown in Figs. 8(a) and 12(a). This is because the magnitude of the equivalent common-mode voltage at high modulation index is large and cannot be ignored. The conventional MPC 2 employs a per-phase model of the MMC that neglects the effect of the common-mode voltage shown in Fig. 8(f), which leads to an inaccurate prediction of the output current and thus affects its control performance.

Fig. 9 shows the output currents $i_{sa}$ (10 A) and their spectrum for the proposed method and conventional methods. The THD results are adopted to evaluate the steady-state performance of the output current. Note that these methods (proposed MPC and conventional MPC 1 and 2) achieve similar performance when the amplitude of the output current is 6 A, with THD of 3.66%, 3.83%, and 3.68%, respectively. However, when the amplitude increases to 10 A in Fig. 9, which means that the MMC operates at high modulation index, both the spectrum and THD results show that the proposed method is better than other methods.

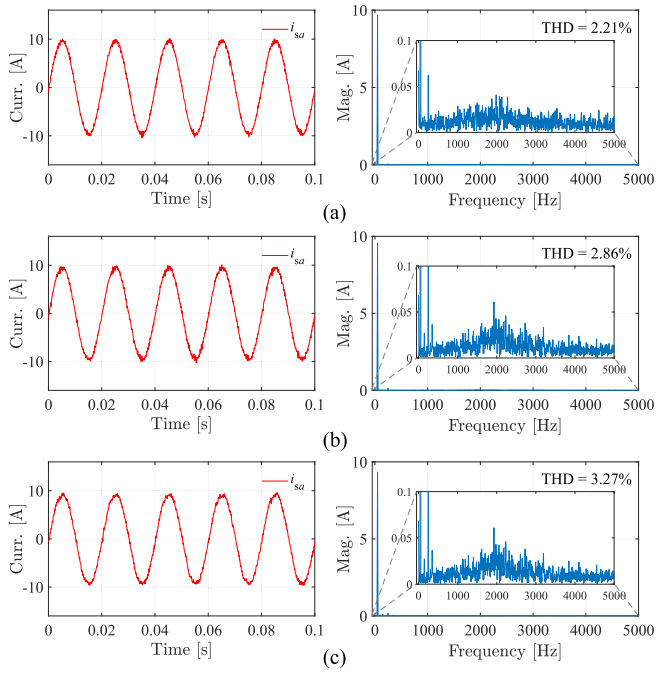


Fig. 9. FFT analysis of output current $i_{sa}$ when the amplitude is 10 A. (a) Proposed MPC. (b) Conventional MPC 1. (c) Conventional MPC 2.

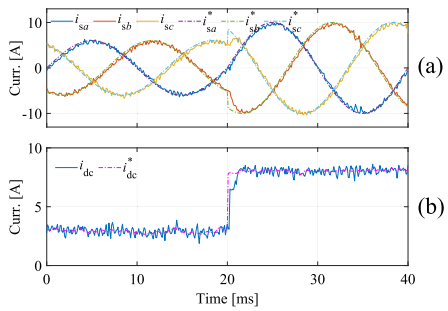


Fig. 10. Detailed waveforms of output currents and the DC-link current of the proposed method. (a) ac-side output currents. (b) dc-link current.

The THD result of the proposed method is only 2.21%, which is an improvement of nearly 23% compared to the THD of 2.86% for the conventional MPC 1. The conventional MPC 2 shows the worst output current performance, with a THD of 3.27%. It is worth noting that an obvious 5th harmonic component can be found in Fig. 9(b) and (c), and it means that the dc-link voltage of the conventional methods cannot be fully utilized. The calculation time and computational burden of these modulated MPC methods are also summarized in Table II. We can find that the conventional method 1, which does not consider constraints, achieves the shortest calculation time as it only needs one iteration to obtain the solution. The maximum calculation time of this method is 17.3 µs. The calculation time of the proposed method only increases about 0.5 µs compared to the conventional method 1 in our platform. Besides, the maximum number of iterations of the proposed method is 7. The calculation time obtained by the conventional MPC 2 is similar to the proposed method. However,

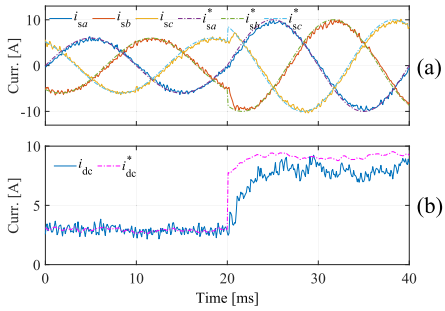


Fig. 11. Detailed waveforms of output currents and the DC-link current of conventional MPC 1. (a) ac-side output currents. (b) dc-link current.

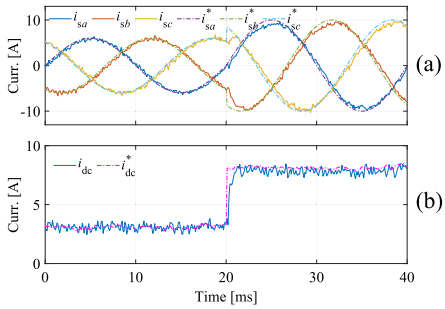


Fig. 12. Detailed waveforms of output currents and the DC-link current of conventional MPC 2. (a) ac-side output currents. (b) dc-link current.

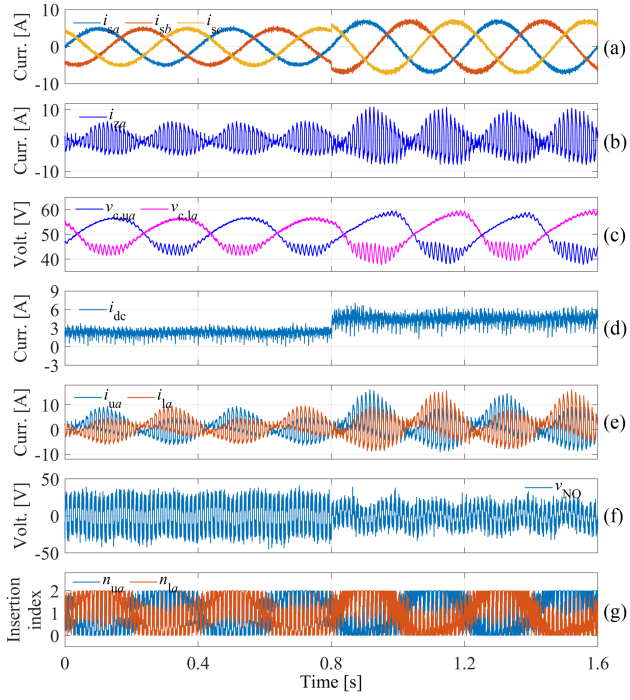


Fig. 13. Step change in ac currents with the proposed modulated MPC combined with the circulating current injection technique at 2.5 Hz. (a) ac-side currents. (b) circulating current of phase a. (c) SM capacitor voltages of the upper and lower arms. (d) dc-link current. (e) upper and lower arm currents of phase a. (f) common-mode voltage. (g) insertion indices of the upper and lower arms.

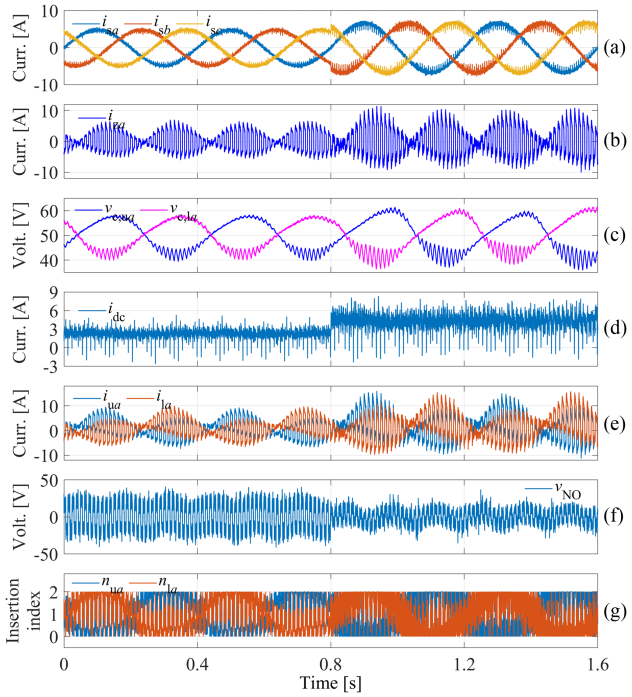


Fig. 14. Step change in AC currents with the conventional MPC 1 combined with the circulating current injection technique at 2.5 Hz. (a) ac-side currents. (b) circulating current of phase a. (c) SM capacitor voltages of the upper and lower arms. (d) dc-link current. (e) upper and lower arm currents of phase a. (f) common-mode voltage. (g) insertion indices of the upper and lower arms.

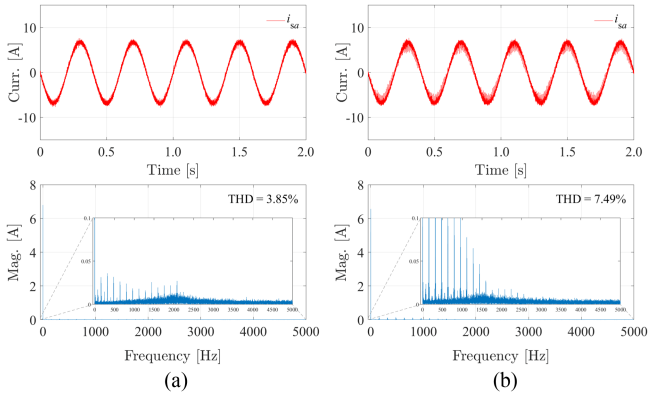


Fig. 15. FFT analysis of output current $i_{sa}$ when the amplitude is 7 A. (a) Proposed method. (b) Conventional method.

as discussed in the introduction, the computational burden of this method is linearly related to the number of SMs per arm, i.e., $3(N+1)$.

In conclusion, conventional modulated MPC methods and the proposed method will present similar control performance at low modulation index as the unconstrained solution is equivalent to the optimal solution of problem (15) in most cases. However, when the MMC system is in transients or high modulation index, the performance of the conventional method is poor as the role of weighting factors has been ignored in this method. Therefore, the control performance of the most important control objective, output currents, will be degraded. Instead, due to a more reasonable allocation of control inputs, the proposed method can improve the steady-state and dynamic performance while retaining the low computational burden characteristic of the conventional modulated MPC method (conventional MPC 1).

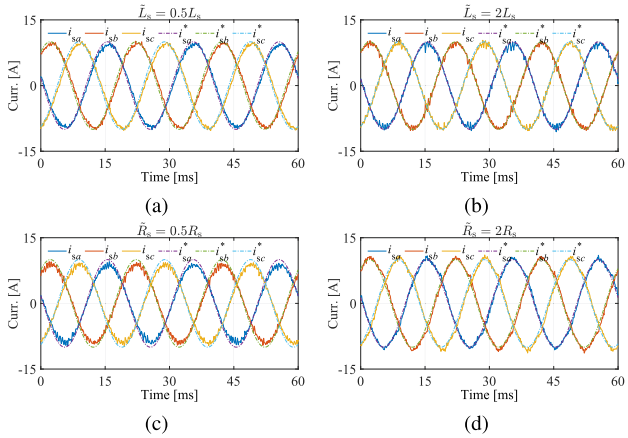


Fig. 16. Results of proposed MPC with mismatched parameters. (a) $\tilde{L}_s = 0.5L_s$. (b) $\tilde{L}_s = 2L_s$. (c) $\tilde{R}_s = 0.5R_s$. (d) $\tilde{R}_s = 2R_s$.

### B. MMC Operates at Low Frequency

The experimental results of the modulated MPC combined with the circulating current injection technique [5] shown in Figs. 13 and 14 can better illustrate the superiority of the proposed method. The implemented weighting factors used in this part are $w_o = 10$, $w_1 = 0.08$, $w_2 = 0.09$, $w_3 = 0.003$. The injected frequency of the injection method is 80Hz.

In Fig. 13, the control performance of the MMC operating at 2.5 Hz controlled by the proposed modulated MPC has been provided. The amplitude of ac-side currents changes from 5 to 7A. Fig. 13 shows that the proposed method can obtain satisfactory steady-state performance of the output currents. Besides, the SM capacitor voltages of the upper and lower arms are balanced and their ripples are suppressed at low frequency. The experimental results of the conventional method are shown in Fig. 14. We can find that when the amplitude of ac-side currents is 5 A, the steady-state performance of ac-side currents is good. However, when the amplitude increases slightly, the output current presents many current spikes at twice the injection frequency. Besides, the ripple in the dc-link current of the conventional method is much higher than that of the proposed method.

FFT analysis and THD results shown in Fig. 15 are utilized to evaluate the ac-side current for both methods. As shown in Fig. 15, the proposed method is far superior to the conventional one, where the THD result of the proposed method is 3.85%, while that of the conventional method is 7.49%.

### C. Parameter Sensitivity Test for the Proposed MPC

In this part, we tested the proposed method for parameter mismatch cases, as shown in Fig. 16. Note that $\tilde{L}_s$ and $\tilde{R}_s$ represents

the ac-side inductance and resistance used in the controller. It can be seen from Fig. 16(a) that when the inductance used in the controller is half of the actual inductance, there is a significant phase lag between the output current and its reference value. When the inductance value is twice the actual value, as shown in Fig. 16(b), the phase lag does not appear, but the output current will oscillate slightly when it reaches the peak value. The experimental results of the proposed method with mismatched resistance can be found in Fig. 16(c) and (d). It can be seen that the output current will slightly smaller than its reference when $\tilde{R}_{\mathrm{s}} = 0.5R_{\mathrm{s}}$. Instead, when the resistance value used in the controller becomes twice the actual resistance, which is shown in Fig. 16(d), the output current will be slightly larger than its reference value and slightly distorted. It is also worth noting that the mismatched resistance value will not cause the phase lag in the output current.

## V. Conclusion

In this work, the limitations of the existing modulated MPC method have been first discussed. It is pointed out that the essence of such methods is to solve the unconstrained solution of an optimization problem. Therefore, when this unconstrained solution is not in the feasible region, it cannot fully consider the importance of different control variables, which leads to a decrease in system performance. To overcome such a problem, the modulated MPC with a bound-constrained QP method has been proposed. Compared with conventional methods, the proposed method performs better in the case of transients and high modulation index due to the use of the optimal solution. Meanwhile, the proposed method also inherits the advantage of low computational burden from modulated methods. Thus, the proposed method is promising for MPC-based MMC systems. Finally, experimental results verify the effectiveness and superiority of the proposed method.

## References


[1] A. Lesnicar and R. Marquardt, "An innovative modular multilevel converter topology suitable for a wide power range," in *Proc. IEEE Bologna PowerTech Conf.*, 2003, vol. 3, pp. 6–11.

[2] M. A. Perez, S. Bernet, J. Rodriguez, S. Kouro, and R. Lizana, "Circuit topologies, modeling, control schemes, and applications of modular multilevel converters," *IEEE Trans. Power Electron.*, vol. 30, no. 1, pp. 4–17, Jan. 2015.

[3] M. Saeedifard and R. Iravani, "Dynamic performance of a modular multilevel back-to-back HVDC system," *IEEE Trans. Power Del.*, vol. 25, no. 4, pp. 2903–2912, 2010, doi: 10.1109/TPWRD.2010.2050787.

[4] M. Hagiwara, R. Maeda, and H. Akagi, "Negative-sequence reactive-power control by a PWM statcom based on a modular multilevel cascade converter (MMCC-SDBC)," *IEEE Trans. Ind. Appl.*, vol. 48, no. 2, pp. 720–729, Mar./Apr. 2012.

[5] B. Li et al., "An improved circulating current injection method for modular multilevel converters in variable-speed drives," *IEEE Trans. Ind. Electron.*, vol. 63, no. 11, pp. 7215–7225, Nov. 2016.

[6] S. Li, X. Wang, Z. Yao, T. Li, and Z. Peng, "Circulating current suppressing strategy for MMC-HVDC based on nonideal proportional resonant controllers under unbalanced grid conditions," *IEEE Trans. Power Electron.*, vol. 30, no. 1, pp. 387–397, Jan. 2015.

[7] J. Wang and P. Wang, "Decoupled power control for direct-modulation-based modular multilevel converter with improved stability," *IEEE Trans. Ind. Electron.*, vol. 66, no. 7, pp. 5264–5274, Jul. 2019.

[8] J. Rodriguez and P. Cortes, *Predictive Control of Power Converters and Electrical Drives*. Hoboken, NJ, USA: Wiley, 2012, vol. 40.

[9] T. Geyer, *Model Predictive Control of High Power Converters and Industrial Drives*. Hoboken, NJ, USA: Wiley, 2016.

[10] J. Qin and M. Saeedifard, "Predictive control of a modular multilevel converter for a back-to-back HVDC system," *IEEE Trans. Power Del.*, vol. 27, no. 3, pp. 1538–1547, Jul. 2012.

[11] M. Vatani, B. Bahrani, M. Saeedifard, and M. Hovd, "Indirect finite control set model predictive control of modular multilevel converters," *IEEE Trans. Smart Grid*, vol. 6, no. 3, pp. 1520–1529, May 2015.

[12] B. Gutierrez and S. Kwak, "Modular multilevel converters (MMCs) controlled by model predictive control with reduced calculation burden," *IEEE Trans. Power Electron.*, vol. 33, no. 11, pp. 9176–9187, Nov. 2018.

[13] A. Dekka, B. Wu, V. Yaramasu, and N. R. Zargari, "Model predictive control with common-mode voltage injection for modular multilevel converter," *IEEE Trans. Power Electron.*, vol. 32, no. 3, pp. 1767–1778, Mar. 2017.

[14] A. Dekka, B. Wu, V. Yaramasu, and N. R. Zargari, "Dual-stage model predictive control with improved harmonic performance for modular multilevel converter," *IEEE Trans. Ind. Electron.*, vol. 63, no. 10, pp. 6010–6019, Oct. 2016.

[15] A. Dekka, B. Wu, V. Yaramasu, R. L. Fuentes, and N. R. Zargari, "Model predictive control of high-power modular multilevel converters - an overview," *IEEE Trans. Emerg. Sel. Topics Power Electron.*, vol. 7, no. 1, pp. 168–183, Mar. 2019.

[16] W. Yang, Q. Song, and W. Liu, "Decoupled control of modular multilevel converter based on intermediate controllable voltages," *IEEE Trans. Ind. Electron.*, vol. 63, no. 8, pp. 4695–4706, Aug. 2016.

[17] J. Huang et al., "Priority sorting approach for modular multilevel converter based on simplified model predictive control," *IEEE Trans. Ind. Electron.*, vol. 65, no. 6, pp. 4819–4830, Jun. 2018.

[18] H. Mahmoudi, M. Aleenejad, and R. Ahmadi, "Modulated model predictive control of modular multilevel converters in VSC-HVDC systems," *IEEE Trans. Power Del.*, vol. 33, no. 5, pp. 2115–2124, Oct. 2018.

[19] Z. Gong, X. Wu, P. Dai, and R. Zhu, "Modulated model predictive control for MMC-based active front-end rectifiers under unbalanced grid conditions," *IEEE Trans. Ind. Electron.*, vol. 66, no. 3, pp. 2398–2409, Mar. 2019.

[20] X. Chen, J. Liu, S. Song, S. Ouyang, H. Wu, and Y. Yang, "Modified increased-level model predictive control methods with reduced computation load for modular multilevel converter," *IEEE Trans. Power Electron.*, vol. 34, no. 8, pp. 7310–7325, Aug. 2019.

[21] J. Yin, J. I. Leon, M. A. Perez, L. G. Franquelo, A. Marquez, and S. Vazquez, "Model predictive control of modular multilevel converters using quadratic programming," *IEEE Trans. Power Electron.*, vol. 36, no. 6, pp. 7012–7025, Jun. 2021.

[22] J. Wang, X. Liu, Q. Xiao, D. Zhou, H. Qiu, and Y. Tang, "Modulated model predictive control for modular multilevel converters with easy implementation and enhanced steady-state performance," *IEEE Trans. Power Electron.*, vol. 35, no. 9, pp. 9107–9118, Sep. 2020.

[23] K. Kunisch and F. Rendl, "An infeasible active set method for quadratic problems with simple bounds," *SIAM J. Optim.*, vol. 14, no. 1, pp. 35–52, 2003.

[24] S. Cui, S. Kim, J. Jung, and S. Sul, "A comprehensive cell capacitor energy control strategy of a modular multilevel converter (MMC) without a stiff dc bus voltage source," in *Proc. IEEE Appl. Power Electron. Conf. Expo.*, 2014, pp. 602–609.

[25] D. Zhou, S. Yang, and Y. Tang, "Model-predictive current control of modular multilevel converters with phase-shifted pulsewidth modulation," *IEEE Trans. Ind. Electron.*, vol. 66, no. 6, pp. 4368–4378, Jun. 2019.

[26] H. W. Kuhn and A. W. Tucker, "Nonlinear programming," in *Proc. 2nd Berkeley Symp. Math. Statist. Probability*, 1950. Berkeley and Los Angeles: University of California Press, 1951, pp. 481–492.



**Xiaonan Gao** (Member, IEEE) received the B.S. and M.S. degrees from the Dalian University of Technology, Dalian, China, in 2013 and 2016, respectively, and the Dr.-Ing. degree from the Technical University of Munich, Munich, Germany, in 2022, all in electrical engineering.

He is currently a Postdoctoral Fellow with the KTH Royal Institute of Technology, Stockholm, Sweden. His research interests include electrical drives, predictive control, multilevel converters, and grid-connected converters.

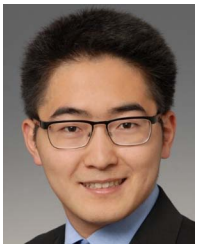

**Wei Tian** (Member, IEEE) received the B.Eng. degree in electrical engineering and automation from Central South University, Changsha, China, in 2012, and the M.Sc. degree in electrical power engineering from RWTH Aachen University, Aachen, Germany, in 2015. He is currently working toward the Ph.D. degree in electrical engineering with the Chair of Electrical Drive Systems and Power Electronics, and the Chair of High-Power Converter Systems, Technical University of Munich, Munich, Germany.

His research interests include power electronics and electrical drives, model predictive control, and modular multilevel converter.

**Qifan Yang** (Member, IEEE) received the B.Eng. degree in electrical engineering from Xi'an Jiaotong University, Xi'an, Shannxi, China, in 2016, and the M.Sc. degree in electrical power engineering in 2019 from the Technical University of Munich, Munich, Germany, where he is currently working toward the Ph.D. degree in electrical engineering with the Chair of Electrical Drive Systems and Power Electronics.

His research interests include optimal control, power electronics, and electrical drives.

**Na Chai** (Member, IEEE) received the B.S. and Ph.D. degrees in electrical engineering from the Harbin Institute of Technology, Harbin, China, in 2014 and 2021, respectively.

From 2021 to 2022, she was a Postdoc with the Chair of Electrical Drive Systems and Power Electronics, and the Chair of High-Power Converter Systems, Technical University of Munich, Munich, Germany. Since 2022, she has been an Associate Professor with the College of Electronic and Information Engineering of Hunan University, Changsha, China. Her research interests include mechanical fault detection based on motor drive systems, model predictive control, and multilevel converters.

**Jose Rodriguez** (Life Fellow, IEEE) received the engineer's degree from the Universidad Tecnica Federico Santa Maria, Valparaiso, Chile, in 1977, and the Dr.-Ing. degree from the University of Erlangen, Erlangen, Germany, in 1985, both in electrical engineering.

He is currently a Director with the Center for Energy Transition, Universidad San Sebastian, Santiago, Chile. Since 1977, he has been the Full Professor and President with the Department of Electronics Engineering, Universidad Tecnica Federico Santa Maria. From 2015 to 2019, he was the President with Universidad Andres Bello, Santiago, Chile. From 2022 to 2023, he was President with Universidad San Sebastian. He has coauthored two books, several book chapters, and more than 700 journal and conference papers. His research interests include multilevel inverters, new converter topologies, control of power converters, and adjustable-speed drives.

Dr. Rodriguez is Member of the Chilean Academy of Engineering. He was a recipient of the number of best paper awards from journals of the IEEE, the National Award of Applied Sciences and Technology from the Government of Chile, in 2014, and the Eugene Mittelmann Award from the Industrial Electronics Society of the IEEE, in 2015. From 2014 to 2022, he was included in the list of Highly Cited Researchers published by Web of Science.

**Ralph Kennel** (Life Senior Member, IEEE) received the diploma and Dr. Ing. (Ph.D.) degrees in electrical engineering from the University of Kaiserslautern, Kaiserslautern, Germany, in 1979 and 1984, respectively.

From 1983 to 1999, he worked on several positions with Robert BOSCH GmbH, Gerlingen, Germany. Until 1997, he was responsible for the development of servo drives. From 1994 to 1999, he was a Visiting Professor with the University of Newcastle upon Tyne, Newcastle upon Tyne, U.K. From 1999 to 2008, he was a Professor of electrical machines and drives with Wuppertal University, Wuppertal, Germany. Since 2008, he has been a Professor of electrical drive systems and power electronics with the Technical University of Munich, Munich, Germany. His research interests include renewable energy systems, sensorless control of ac drives, predictive control of power electronics, and hardware-in-the-loop systems.

Dr. Kennel is a Fellow of the IET and a Chartered Engineer in the U.K. He is an Associate Editor for IEEE TRANSACTIONS ON POWER ELECTRONICS. He is a Treasurer of the Germany Section of IEEE.

**Marcelo Lobo Heldwein** (Senior Member, IEEE) received the B.S. and M.S. degrees from the Federal University of Santa Catarina (UFSC), Florianópolis, Brazil, in 1997 and 1999, respectively, and the Ph.D. degree from the Swiss Federal Institute of Technology (ETH Zurich), Zurich, Switzerland, in 2007, all in electrical engineering.

He is currently the Head of the Chair of High-Power Converter Systems, TUM School of Engineering and Design, Technical University of Munich (TUM), Munich, Germany. From 1999 to 2003, he was with industry, including research and development activities with Power Electronics Institute, Florianópolis, Brazil, and Emerson Network Power, Brazil and Sweden. From 2007 to 2009, he was a Postdoctoral Fellow with the ETH Zurich and the UFSC. From 2010 to 2022, he was a Professor with the Department of Electronics and Electrical Engineering, UFSC. His research interests include power electronics, advanced power distribution technologies, and electromagnetic compatibility.

Dr. Heldwein is a Member of the Brazilian Power Electronic Society (SOBRAEP) and a Member of the Advisory Board of PCIM Europe.